Experimental study of the droplets evolution upon impulse spray formation

A.N. Ishmatov*, B.I. Vorozhtsov
Laboratory of Physics of High-Energy Materials Energy Conversion,
Institute for Problems of Chemical and Energetic Technologies of the Siberian Branch
of the Russian Academy of Sciences (IPCET SB RAS), Russia
ishmatoff@rambler.ru

Abstract

The impulse formation of sprays, considering the evolving droplets in the dispersed flow, has experimentally been studied. The spray formation process was simulated in laboratory conditions by applying a modified hydrodynamic tube-type device using a gas-generating pyrotechnic charge to intensify atomization. For comprehensive study using both known and dedicated technique. The research revealed a limitation for measurements by the low-angle light scattering method due to the multiple light scattering in the dispersed flow at the initial step of the flow formation. To diminish the effect, a method of the optical path decrease by a factor of 2 was applied. On atomizing NaCl solutions by the 'salt residue' procedure, we found that the morphology of salt residue particles reflect the 'marks' of processes occurring during the atomization. The estimation of the particles morphology showed a highly increased evaporation rate within the first several milliseconds after the atomization. The general picture of the droplets evolution upon the impulse spray formation is described.

Introduction

This research was performed for solving problems of the impulse spray formation. The work is urgent in view of the necessity to investigate the spray generation processes for prompt neutralization and deactivation of noxious aerosol and gas emissions as well as for suppressing fires and blast waves in coal mines. The efficiency of utilizing hydrodynamic tube-type devices for the impulse atomization of liquids, generation of aerosol barriers and dispersed flows was demonstrated previously [1–4]. Atomization by this type of a device is based on methods of utilization of physical effects arising in liquid under conditions of shock waves and when pressure rapidly changes [5]. The effectuation of those methods implies the existence of many gas bubbles distributed in the liquid phase. Upon high-speed impulse outflow of a liquid, the gas pressure in bubbles is almost instantly dissipated to the ambient pressure, the gas bubbles rapidly expand and the effect of explosive boiling arises that is accompanied by high-amplitude pressure impulse and by turbulization of liquid boundary layers. This set of phenomena and high velocity of liquid emerging in a divergent flow from nozzle results in effective liquid atomization.

The process of liquid atomization by hydrodynamic tube-based devices can be intensified in various ways:

- Cavitating a liquid upon shock loading, for instance, upon piston punch [3];
- Using compressed gas for mixing a liquid under high pressure and impulse ejection of the resultant vapor–liquid mixture within a very short time (several ms) [1];
- Using a gas-generating pyrotechnic charge [2, 4, 6] that burns to cause a shock wave leading to the liquid caviation, and the resultant gas is mixed with the liquid to gasify it;
- Atomization of the overheated liquid the ejection of which causes boiling throughout the volume, and the resultant vapor, breaking the jet, contributes to the further spray formation [7].

The gas-generating pyrotechnic charge method allows combination of shock action mechanisms with application of high-pressure gas, thereby enhancing the atomization efficiency. In addition, the use of a pyrotechnic charge as a source of energy in impulse-type atomizers results in a sufficient amount of energy within a short period of time. The pyrotechnic charge occupying a small volume, which affords the possibility to design autonomous aerosol screening systems that are especially sought-for in coal mines. Requirements for devices that generate aerosol screens are increasingly getting more severe every year. Accordingly, the role of theoretical and experimental studies of the impulse spraying principles is growing. More important and virtually essential is the knowledge of the features of processes that occur as a result of influencing factors such as flow turbulence, cavitation, and air friction in the least investigated breakup regime of liquid jets classified by Ohnesorge [8]. Some aspects of deriving mathematical models and obtaining analytical dependences for the description of impulse liquid atomization processes with due account for cavitation phenomena were previously reported [2, 3, 6, 9]. The issue of investigating the spray formation, taking into account the evolving droplets in the dispersed flow, remains urgent. The further development of the impulse atomization theory is apparently impossible without adequate experimental data on the complicated processes of atomization and spray formation.

This research is aimed at developing the experimental base and investigating the evolution of droplets in the dispersed flow upon the impulse spray formation.

2 Experimental complex, Measurement Procedures, and Methods

The impulse spray formation process was simulated in laboratory conditions by applying a device in the form of a modified hydrodynamic tube (Figure 1) [2]. In the atomizer, which represents a hydrodynamic tube, the gas-generating pyrotechnic charge is separated from the liquid by a waterproof diaphragm. The shock waves resulted from the charge burning causes the liquid cavitation, and the generated gas is mixed with the liquid to consequently bring about a foamed structure that outflows with a high velocity through the nozzle. The limiter serves for adjusting the spray shape and nozzle cross-section area [2, 10]. The liquid spray formation occurs once, within about a few ms, under nonstationary conditions at high liquid ejection velocities. The flow issuing from atomizer is conical and hollow. The schematic in Figure 2 illustrates the experimental setup designed for the present study taking into account the impulse liquid atomization features that impose significant limitations on measurements.

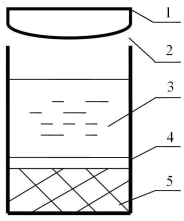

1 – limiter; 2 – nozzle; 3 – liquid; 4 – casing; 5 – pyrotechnic charge

Figure 1 Atomizer schematic [2].

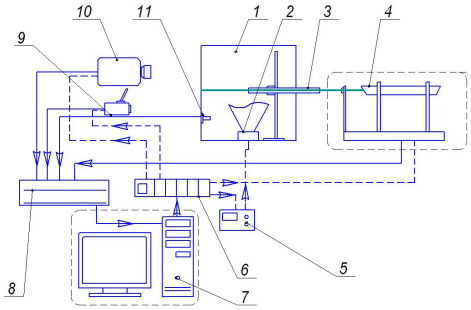

(a)

(b)

1 – experimental box; 2 – atomizer; 3 – protective tube; 4 –laser measurement setup; 5 – initiation unit; 6 – synchronization unit; 7 – PC; 8 – information acquisition unit; 9 – thermal imager; 10 – high-speed video camera; 11 – humidity sensor

Figure 2 A block diagram (a) and general view (b) of the experimental complex.

We used the standard technique and those specially designed with due account for the specific character of the research.

2.1 Digital image and video capture

Visualization was carried out with a CCD video camera with adjustable frame rates up to 10,000 frames per second and exposure adjustable times between 10^{-9} and $33 \cdot 10^{-3}$ s. The number of pixels of the CCD images is inversely proportional to the exposure time with a maximal resolution of 1280 x 1000 (pixel size 12 x 12 μm) and the dynamic range of the camera was 10 bit. A standard c-mount lens with 50 mm focal length (maximum aperture *f*/4) was used to focus images of the flow features on the CCD sensor. All observed flow features were illuminated by two 1 000 W continuous light sources. The video recording results are provided in the form of frame sequences (video sequence) that are used to estimate the dynamics of spray formation and evolution.

2.2 Infrared camera

To evaluate thermal fields in the spray, an infrared camera was used. The camera specifications are as follows: uncooled FPA microbolometer detector; effective resolution 384×288 pixels (pixel size 35 μm); spectral range 8–14 μm; thermal sensitivity 0.08°C; field of view/focus 22°×16°/35 mm; frame frequency 24 fps.

Accurate measurements are rather difficult to perform because the spray is semitransparent and rapidly varying. Upon measuring temperature of a body in the infrared range, one should take account of the object's intrinsic radiation, the radiation passed through the object, and the radiation reflected by the object. To minimize errors in measurements, the experiment was conducted in a closed experimental box coated with black dull paint and do not let the thermal radiation through. The spray surface exhibits Lambertian reflectance, light falling on it is scattered such that the apparent brightness of the surface to an observer is the same regardless of the observer's angle of view. The absorptivity was taken equal to one, namely, to the water absorption coefficient in the thermal imager spectral range (8–14 μm). The temperature measurements were performed in the spray with the highest concentration in order to avoid a possible influence of the thermal radiation passed through the spray.

2.3 Laser Measurement Setup

The laser measurement setup [11] based on the low-angle laser light scattering method (LALLS) using a line of sight forward diffraction technique was employed to study the droplets dispersiveness parameters and spray evolution. The setup enables remote contactless measurements of the dispersiveness and concentrations of droplets in the spray. The method comprises a laser providing a Gaussian beam of 1.5 mm diameter at the wavelength of 631 nm and power of about 5 mW. The intensiveness of the radiation scattered on aerosol particles (scattering indicatrix) was recorded by 8 photodiode elements at angles from 0.3° to 20° in the plane perpendicular to the

laser beam. The recording frequency of measured data was 100 kHz. The error in measuring the scattering indicatrix did not exceed ± 5 % of the true value. The optical path length was 1 m. The scattered radiation signal after it had been recorded by the photodiodes was processed with an ADC board installed in a PC. Then, by numerically solving a series of direct problems of aerosol optics and comparing the experimental scattering indicatrix with the calculated, we restored the particle size distribution function. The generalized gamma distribution was chosen as a basis function [11]:

$$f(D) = aD^{\alpha} \exp(-bD),$$

where a >0 – normalizing factor; α, b – distribution parameters; D – particle diameter.

Application of this function to fit experimental drop size distribution reported convincing agreements for sprays produced by a high-pressure atomizer [12].

2.3.1 Optimization of the LALLS method to study dense flows

When the probe laser radiation passes through the spray volume (near the nozzle region), there may occur an effect of multiple light scattering by the particles at the initial stage of the impulse spray formation [12, 13], which makes measurements impossible. The effect of the multiple light scattering by the particles during the restoration of the distribution function can be disregarded in case the condition for the dispersed medium optical thickness, τ, is fulfilled [14]: $\tau < 1.5$.

$$\tau = \ln(I_0 / I) = k\, l_s,$$

where I – the radiation intensity after passing through the spray volume; I_0 – the radiation intensity when the particles are absent in the volume; k – the attenuation index of the medium; l_s – the optical path length (m).

To minimize the effect of the multiple scattering, it was suggested to employ a device in the form of a protective tube twice reducing the optical path length, as shown in Figure 3. The protective tube is placed in such a way as to isolate the probe laser beam on the half of the dispersed flow. Measurements without loss of information about the flow are possible when the flow is symmetric.

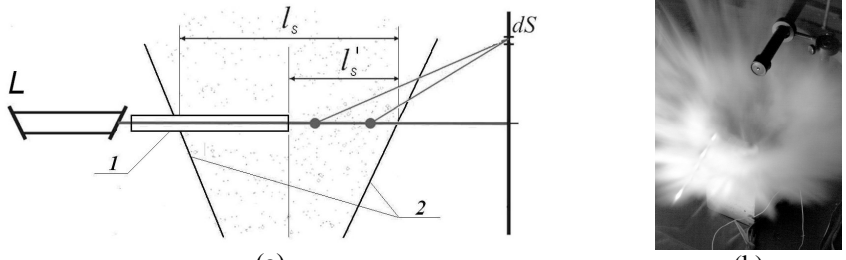

(a) (b)

L – Laser; 1 – protective tube; 2 – boundaries of the aerosol cloud; *dS* – area on which the radiation comes when scattered at different angles; l_s – optical path length without using the protective tube; l_S' – optical path length using the protective tube.

Figure 3 Diagram (a) and general view (b) of the experimental setup.

When the optical path length $l_S' = l_S / 2$, the optical thickness, τ', for the same dispersed medium is also decreased by a factor of 2:

$$\tau' = \ln(I_0 / I') = k\, l_s' = \tau / 2,$$

where I' – the intensity of the radiation after passing through the spray volume at the optical path length l_S'.

Thus, using the protective tube (twice decrease in optical path length, $l_S' = l_S/2$) makes it possible to enhance the measurement threshold in the droplet cloud from $\tau < 1{,}5$ to $\tau < 3$. The influence of the optical path length decrease on the measurement results is taken into account by numerical methods upon processing measurement data [11].

2.4 The Salt Residue Method

The LALLS method permits measurements with a small time step directly in the flow, which is urgent with respect to the evolution study of droplets formed. The method is hard to use for the study of droplets at the initial stages of the flow formation under conditions of increased density and nonstationarity of the dispersed flow. There exists a problem of selecting a measurement region in the flow because it is difficult to estimate the distance at which the dispersion stage still proceeds; the coagulation of droplets is not excluded and, in addition, their shape may be other than spherical. In case a larger distance is chosen beforehand, the measurement results will reflect the picture with a lapse of time in which the size of droplets may be changed by evaporation.

To perform the work, an experimental method has been suggested that also permits using the whole ensemble of droplets resulting from the atomization. The method consists in atomizing NaCl solutions, evaporating the

solution droplets, and subsequently determining the disperse composition of droplets in the spray from the study results for the dry salt residue. The method is informative so far as the dry residue particle size is directly associated with the content of a nonevaporable impurity in the droplet, and the disperse composition of the initial droplets is defined:

$$D_1 = D_2 \sqrt[3]{C_m \, \rho_d / \rho_{imp}} , \quad (1)$$

where D_1 – the diameter of the initial droplet; D_2 – the equivalent diameter of the final particle; ρ_{imp} – the solute density; C_m – the relative mass concentration of the solute in solution; ρ_d – the droplet density.

Equation (1) was derived from the equality condition between mass contents of the nonevaporable impurity in the droplet of the initial solution and the particle mass after complete evaporation of the solvent:

$$m_{imp} = m_2; \; C_m \, \rho_d \, \pi D_1^3 / 6 = \rho_{imp} \pi D_2^3 / 6 ,$$

where m_{imp} – the impurity mass in the solution droplet, m_2 – the mass of the final particle.

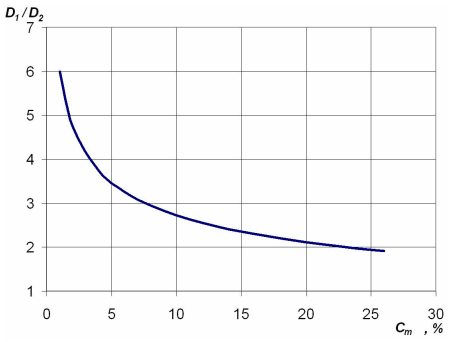

Figure 4 The curve showing D_1/D_2 relation versus NaCl solution concentration.

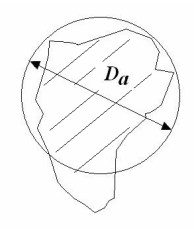

Figure 5 Equivalent particle diameter.

The calculation of the relation between the size of the initial droplets and the diameter of the final particles when a NaCl solution of different concentration is evaporated is exemplified in Figure 4. The equivalent particle diameter is used in view of the fact that the shape of the particles may be other than spherical and represents the diameter of the equivalent sphere, D_a, the area of which is equal to the area of the particle projection (Figure 5). For NaCl, ρ_{imp} =2165 kg/m^3, depending on its content in solution, ρ_d, is found from Table 2 [15].

Table 2 Density of aqueous NaCl solutions

Parameter	Value									
C_m, %	2	6	10	14	16	18	20	22	24	26
ρ_d, kg/m^3	1012	1041	1071	1101	1116	1132	1148	1164	1180	1197

The «salt residue» method does not require sophisticated mechanisms to be developed and special preparation of samplers, and admits of using a comprehensive approach (several research methods are employed simultaneously), which is particularly topical for maximal informativeness of measurements in one experiment. For instance, the application of electron microscopy methods to study liquid droplets faces difficulties but is quite possible to study solid residue particles.

3 Results and Discussion

The 1 m^3 measurement box was used to examine the spray of the selected substances—water and aqueous salt solutions. If necessary, desired temperature and humidity were provided. The experimental conditions were as follows:

- For atomization, distilled water and 20% NaCl solution (1–10 g) were used;
- Ambient air temperature: 293 K;
- Video recording frame rate: 3000 Hz;
- Frame exposure time: 326 μs.

As per conditions of the optimal atomization mode [2, 6], the spray formation was performed under the working pressure of ~120 bar, the opening angle of the spray being 90°.

3.1 Spray Evolution Dynamics

The high-speed video recording of the impulse atomization (Figure 6) showed that the spray has a conical symmetric shape, the liquid ejection from the atomizer is completed in 3 ms, the mean flow rate corresponds to ~200 m/s, the cloud is formed in 8 ms. The dynamics of increase in the cloud volume when ejected was evaluated from the variation of the geometrical parameters, and a region to measure the disperse characteristics by the laser setup using the LALLS method was selected. In the case of the impulse atomization of liquids, the liquid release rate has to be spoken about quite conditionally since it would be more correct to consider the field of rates in the spray, which is governed by the impulse pressure rise due to the pyrotechnic charge actuation and by

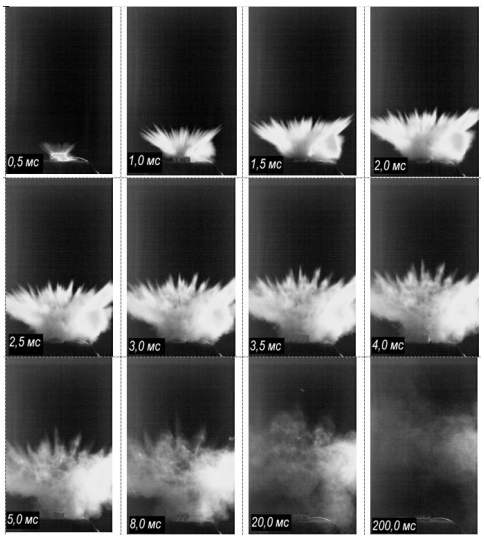

Figure 6 Visualization of impulse spray formation.

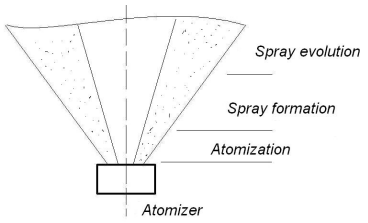

Figure 7 Flow division schematic.

the pressure decrease during the liquid outflow. According to the experimental findings and theoretical aspects of the liquid atomization [16, 17], it is possible to concretize the formation and evolution stages of a cloud of fine droplets upon the impulse atomization:

- Atomization of a cavitated liquid (~3 ms);
- Spray formation under conditions of high-speed outflow (~8 ms);
- Spray evolution (over 8 ms).

The impulse dispersed flow can be considered as a conical body of rotation and is conditionally divided into zones, as shown in Figure 7. Strongly turbulized impulse flows at distances exceeding 0.1 m give rise to the crisis of drag resistance (resistance to the movement of droplets in the flow appears to be 4–7 times smaller than that of a separate droplet) [18, 19] and, accordingly, the probability of the secondary atomization of a droplet in such a flow is minimal. And from the viewpoint of the eventual result, the droplet formation process due to the primary and secondary atomization is logical to consider in one zone (the atomization zone) as the primary atomization occurs almost near the nozzle and the secondary one is limited by small distances of about 0.1 m from the nozzle. The spray formation zone is characterized by high velocities of the dispersed flow. The length varies from 0.1 m, depending on the dispersed liquid volume and the spray shape. The final zone corresponds to the spray evolution zone where droplets are in equilibrium and the spray evolution is due to evaporation, condensation, coagulation, and gravitational sedimentation of the particles.

3.2 Measurement Data by the LALLS Method

The measurements of distilled water spray by LALLS method were performed in the closed experimental box. The spray formation region (distance of 0.15 m from the nozzle) and the spray evolution region (distance of 0.3 m from the nozzle) were selected for our study. The experimental study showed that under the above conditions the measurements with using the protective tube can be done without due account for the effect the multiple light scattering, starting from 8 ms, whereas in case the protective tube is not used, the measurements can be done starting from 50 ms (Figure 8).

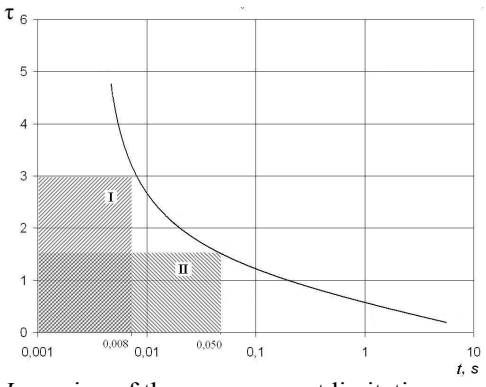

I – region of the measurement limitation using the protective tube; *II* – region of the measurement limitation without the protective tube.

Figure 8 The optical thickness variation in the experiment.

The disperse characteristics for a time period up to 8 ms cannot be measured due to the high optical thickness of the spray. However, the usage of the protective tube allows studying the spray evolution straight from the moment after the spray formation. The study of the dispersiveness evolution at the center of the spray (distance of 0.3 m from the nozzle) showed that the liquid spray has almost constant characteristics, starting from 8 ms up to 1 s of the evolution. A considerable change in the dispersiveness of the droplets (weighted average mean diameter, D_{43}, was used to estimate the dispersiveness) was observed at the boundary of the spray (distance of 0.15 m from the nozzle—the lower boundary). This is associated with the unstable structure of the spray due to circulation and evaporation: droplets closer to the boundary are more liable to evaporation than those present at the center. In addition, the temperature measurement in the spray showed 291 K, which corresponds to the temperature of the wet bulb thermometer in the same conditions and indicates the ongoing droplet evaporation.

Table 3 The change in D_{43} upon atomizing distilled water.

Parameter	Value								
t, s	0.008	0.02	0.03	0.040	0.1	0.2	1.0	2.0	6.0
D_{43}, μm, 15 cm from the nozzle	15.9	16.6	16.5	17.5	17.2	16.9	10.8	8.8	8.5
D_{43}, μm, 30 cm from the nozzle	16.8	16.1	16.5	16.7	16.5	17.0	17.3	14.5	13.8

Thus, it was shown that the liquid spray produced by the impulse atomization is rather stable and stationary at the spray evolution stage. The life time of the spray apparently depends on the occupied volume, atomized liquid weight, air humidity, heat exchange, and convection flows, which can happen in real conditions.

3.3. Measurement Data by the Salt Residue Method

The salt residue method was employed to provide a possibility of estimating sizes of initial droplets. The sampling was carried at the bottom of the closed experimental box for 24 h.

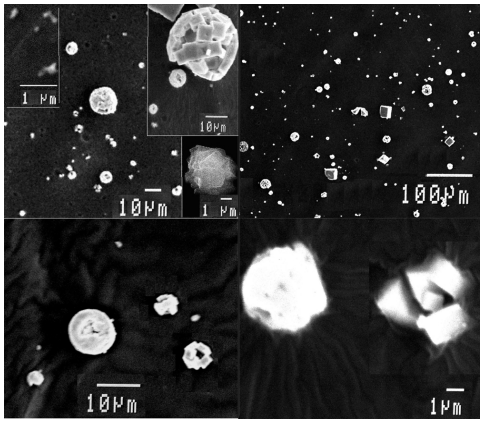

Figure 9 Particles of the dry salt residue resulted from the impulse atomization.

The LALLS method to investigate the initial stages of the dispersed flow formation being inappropriate, as is shown above, the estimation of the sizes of the initial droplets is important because high ejection velocities may govern a high velocity of the evaporation [17, 20], which may lead to a significant change in their sizes. As a result of the electron microscopy study of the droplets formed upon the impulse atomization of a NaCl solution, it was found that their morphology may be different – solid polycrystalline/monocrystalline structures and hollow spheroids which are also distinct in structure and sizes of crystals constituting their surface (Figure 9). The different morphology causes errors in estimating the initial droplets sizes since the accurate calculation requires the precise determination of the salt residue weight. In other words, in order to obtain the distribution of droplets by the salt residue, it is needed to determine the weight of every separate particle in view of their different morphology.

3.4 Evaluating the Processes Leading to the Formation of Salt Residue Particles

When a solution droplet moves, a number of various processes arise. To demonstrate the effect degree of these processes on the formation of the salt residue particles, the characteristic times were estimated [21]:

$$t_1 = \frac{\rho_d D^2}{18\mu_g};\ t_2 = 0{,}25D^2/æ;\ t_3 \approx \frac{\rho_d D^2}{\mu_d};\ t_4 = \frac{18\,\mu_g\, H}{\rho_d\, D^2 g};\ t_5 = \frac{\rho_d\, D^2}{8D_{AB}(C_S - C_\infty)};\ t_6 = \frac{D^2}{4D'_{AB}},$$

where t_1 – the characteristic time of the velocity relaxation of the droplets; t_2 – the characteristic time of the temperature equalization in the droplet; t_3 – the characteristic time of the attenuation of nonstationary perturbation in the droplet due to the viscous energy dissipation; t_4 – the characteristic time of the gravitational sedimentation of the droplet; t_5 – the characteristic time of the droplet evaporation; t_6 – the characteristic time of the solute diffusion; ρ_d – the density of the matter of the particles; D – the droplet diameter; μ_g – the air dynamic viscosity coefficient; æ – the temperature conductivity coefficient; μ_d – the dynamic viscosity coefficient of the droplet matter; H – the height of the lower boundary of the aerosol cloud (distance from the chamber bottom to the cloud boundary); g – the free fall acceleration; D_{AB} – the diffusion coefficient of the liquid vapors in the air; C_S – the concentration of the equilibrium vapor; C_∞ – the vapor concentration in space; D'_{AB} – the diffusion coefficient of the solute in solution.

As an example, let us consider 20% NaCl solution droplets in the size range from 1 μm to 30 μm under atmospheric pressure at 293 K and 50% relative air humidity, with $\mu_g = 18{,}27\cdot10^{-6}$ Pa·s, $\mu_d = 1{,}002\cdot10^{-3}$ Pa·s, $D'_{AB} = 1{,}1\cdot10^{-9}$ m^2/s, D_{AB}, $= 0{,}23\cdot10^{-4}$ m^2/s, $\rho_d = 1000$ kg/m^3, $C_S = 0{,}02$ kg/m^3, $C_\infty = 0{,}01$ kg/m^3, æ$=1{,}4\cdot10^{-7}$ m^2/s [22], H=0,3 m. The calculation results are collected in table 4.

Table 4 Characteristic times of the droplet evolution process

Parameter	Value					
D, μm	1	5	10	15	20	30
t_1, s	$0.3\cdot10^{-5}$	$8.8\cdot10^{-5}$	$35.4\cdot10^{-5}$	$79.6\cdot10^{-5}$	$141.5\cdot10^{-5}$	$318.5\cdot10^{-5}$
t_2, s	$0.2\cdot10^{-5}$	$4.4\cdot10^{-5}$	$17.8\cdot10^{-5}$	$40.2\cdot10^{-5}$	$71.4\cdot10^{-5}$	$160.7\cdot10^{-5}$
t_3, s	10^{-6}	$2.5\cdot10^{-5}$	10^{-4}	$0.2\cdot10^{-3}$	$0.4\cdot10^{-3}$	$0.9\cdot10^{-3}$
t_4, s	10^4	$0.4\cdot10^3$	$0.1\cdot10^3$	44.7	25.2	11.9
t_5, s	$5.6\cdot10^{-4}$	$1.4\cdot10^{-2}$	$5.4\cdot10^{-2}$	0.12	0.216	0.489
t_6, s	$2.2\cdot10^{-4}$	$0.5\cdot10^{-2}$	$2.3\cdot10^{-2}$	$5.1\cdot10^{-2}$	$9.0\cdot10^{-2}$	0.204

It is evident that the salt diffusion in the droplet volume determines the process of crystal formation. The evaluation of the characteristic times indicates that the evaporation process is comparable in dynamics to diffu-

sion, and the processes of velocity relaxation, temperature equalization, and perturbations in the droplet go fairly rapidly and may be disregarded. The gravitational sedimentation of the particles can also be neglected in view of its incomparably long evolution. The formation of the salt residue can be described as follows: when atomizing a solution, the salt concentration near the surface is increased by the evaporation of the solvent form the droplet surface; the salt diffuses toward the droplet center and once a certain concentration value is achieved, there takes place crystallization to form a condensed residue. The formation of the residue determines the particle morphology and comprises two periods. In the first period, there is formed a primary structure of the droplet. Assume that once the salt concentration reaches some critical value of oversaturation, C_{cr}, on the solution droplet surface, the nucleation of the crystal takes place. In this case, depending on the evaporation rate and the salt diffusion rate in the droplet volume, a few options are possible.

1. The nucleation of one of several crystals to form a solid particle. In case of a relatively slow evaporation and high-speed diffusion of the salt, when C_{cr} is reached on the droplet surface, the salt concentration in all the volume is close to the equilibrium concentration C_*..
2. The nucleation of a plurality of crystals on the droplet surface to generate a hollow particle.

In the second period, the residual solvent is evaporated and the salt is settled down on the initially formed crystals to form solid or hollow particles. The formation of the solid particles is defined by the condition [23]:

$$t_6 / t_5 < 0,6 . \quad (2)$$

It follows from Table 4 that condition (2) is fulfilled and solid particles must be formed. From the morphology of the particles obtained in the experiment, it may be concluded that the evaporation velocity of the droplets upon the impulse atomization is somewhat higher, that is, conditions of fast evaporation are provided. The evaporation velocity increment is due to the airflow of the droplets in the high-speed dispersed flow during the spray formation. On the basis of theoretical considerations confirmed by the measurement of the diameter decrease velocity of the droplets exposed to airflow, the evaporation velocity under such conditions can be represented by the equation [17]:

$$I_F = I_S K_F ,$$

where I_F – the evaporation rate of the droplets exposed to airflow; I_S – the evaporation rate of the stationary droplets; K_F – the mass-transfer coefficient taking into account an increase in the evaporation rate of the droplets being in motion.

$$K_F = 0,78 + 0,308\left(\mathrm{Re}\right)^{\frac{1}{2}}\left(\mathrm{Sc}\right)^{\frac{1}{3}}, \text{ for } \mathrm{Re} \geq 25 , \quad (3)$$

where $\mathrm{Sc} = (D_{AB}\ \rho_g / \mu_g)^{-1}$ – Schmidt number; $\mathrm{Re} = \rho_g u D / \mu_g$; ρ_g – the air density; u – the velocity of the airflow to which the particles are exposed.

As follows from (3), the particles present under the airflow conditions have K_F greater than 1. In other words, the evaporation rate of the droplets when exposed to airflow will be higher than those of the droplets present under stationary conditions. The airflow effect has an impact on the evaporation only at the first stage of the impulse spray formation when the release velocities are high. The droplet formation in the dispersed flow has rather a complicated character expressed in the particles interaction and decrement of the resistance of the movement of a group of the particles compared to the resistance of a separate particle [18, 19]. In view of the above listed reasons, it is yet impossible to give an accurate description of the evaporation process in the impulse flow.

Thus, the morphology of the salt residue particles upon the impulse atomization indicate that there are provided conditions of the fast evaporation of the droplets owing to high release velocities (~200 m/s). The characteristic time of the velocity relaxation of the droplets movement is much lower than the evaporation time but during this time the evaporation is much faster than the stationary evaporation of the same droplets, that is, the evaporation process in this interval of time is faster than diffusion. Eventually, the salt concentration on the droplet surface is closer to the oversaturation value and even such a short time is enough for the initial formation of a crust of crystals and further formation of hollow spherical particles due to the secondary sedimentation of NaCl on the inner surface of the salt crust.

Summary and Conclusions

As a consequence of the study, a general picture has been described for the droplet evolution upon the impulse atomization of liquids with the aid of the experimental simulation of the impulse dispersion under laboratory conditions by applying a modified hydrodynamic tube-based device using a pyrotechnic charge. Considering the specific character of the impulse liquid atomization, we developed an experimental research complex comprising both the known and dedicated methods and procedures. The study revealed a limitation on measurements by the low-angle light scattering method, which is caused by the multiple light scattering in the dispersed flow at the initial stage of its formation. The experimental investigation showed that under the used conditions the measurements by the devised procedure using the protective tube without due account for the effect of the multiple light scattering by the particles can be run starting from 8 ms after the onset of the liquid atomi-

zation, whereas the protective tube is not employed, the measurements can be performed starting from 50 ms. The liquid spray produced by the impulse atomization was found to be fairly stable and stationary at the spray evolution stage. In the electron microscopy characterization of the particles formed upon the impulse atomization of a 20% NaCl solution, it was found that their morphology may be different, that is, solid polycrystalline/monocrystalline particles and hollow spheroids. In other words, the salt residue particles are a sort of 'artifacts' reflecting the 'marks' of processes that occurred during atomization. The evaluation of the particles morphology showed that the droplets at the first several milliseconds after the formation underwent various interactions with the environment and their evaporation rates were significant. In addition, when designing and testing impulse-type atomizing devices, the existence of hollow spheroids can serve as an 'indicator' of a maximally effective interaction between the dispersed flow and the environment at the initial stage of the flow formation and, hence, of a more effective liquid atomization.

Acknowledgement

The research was performed under partial support of the Russian Foundation for Basic Research (grant no. 11-01-90701).

References

[1] Bogdevicius, M., Suslavicius, V., *Transport and Telecommunication* 19-2: 342-349 (2006).
[2] Vorozhtsov, B.I., Kudryashova, O.B., Ishmatov, A.N., Akhmadeev, I.R., Sakovich, G.V., *Journal of Engineering Physics and Thermophysics* 83-6: 1149-1169 (2010).
[3] Kedrinskiy, V.K, *The Gas Dynamics of Explosion: Experiment and Models* (in Russian), SB RAS Publisher, Novosibirsk 435, 2000.
[4] Shkarabuga, G.N., Zakhmatov, V.D., Scherbak, N.V., *Issues of Defense Technology*. *Series 16: Technical Means of Counteractions against Terrorism* 7–8: 76–84 (2010).
[5] Dolinskii, A.A., *Journal of Engineering Physics and Thermophysics* 69-6: 653-663 (1996).
[6] Kudryashova, O.B., Vorozhtsov, B.I., Muravlev, E.V., Akhmadeev, I.R., Pavlenko, A.A., Titov, S.S., *Propellant, Explosives, Pyrotechnic* 36: 524-529 (2011).
[7] Ostakh, S.V., Akimov, M.N., RU Patent 2067465, *A Fire-Extinguishing Method* (1996).
[8] Ohnesorge, W.V., *Math.Mech* 16: 355-358 (1936).
[9] Stebnovskii, S.V., *Combustion, Explosion, and Shock Waves* 44-2: 228-238 (2008).
[10] Kudryashova, O.B., Vorozhtsov, B.I., *Izvestia VUZov. Physics* (in Russian) 8-2: 107–114 (2008).
[11] Kudryashova, O.B., Akhmadeev, I.R., Pavlenko, A.A., Arkhipov, V.A., Bondarchuk, S.S., *Key Engineering materials* 437: 179-183 (2010).
[12] Boyaval, S., Dumouchel, C., *Particle & Particle Systems Characterization* 18-1: 33-49 (2001).
[13] Hendrik Christoffel van de Hulst, *Light Scattering by Small Particles (Structure of Matter Series)*, Chapman & Hall 470, 1957.
[14] Golubev, A.G., Yagodkin, V.I., Optical Measurement Methods for Aerosol Dispersivness (in Russian), *TSIAM Proceedings* 828: 21 (1978).
[15] Ivanov, V.M., Semenenko, K.A., Prokhorova, G.V., Simonov, Ye.F., *Analytical Chemistry of Sodium* (in Russian), M: Nauka Publisher 245: 1986.
[16] Liu H. Science and Engineering of Droplets - Fundamentals and Applications, William Andrew Publishing: Noyes 508, 2000.
[17] Lefebvre, A.H., *Atomization and Sprays*, Hemisphere, New York 417, 1989.
[18] Simakov, N.N., *Technical Physics* 49-2: 188–193 (2004).
[19] Loitsyanskiy, G.G., *Mechanics of Liquid and Gas*, M: Nauka 736, 1978.
[20] Fuks, N.A., *Evaporation and Growth of Droplets in Gaseous Medium*, M: Mir Publisher 314, 1986.
[21] Vasenin, I.M., Arkhipov, V.A., Butov, V.G., Glazunov, A.A., Trofimov, V.F., *Gas Dynamics of Two-Phase Flows in Nozzles* (in Russian), TGU Publisher 264, 1986.
[22] Reid, R.C., Sherwood, T.K., Properties of gases and liquids: their estimation and correlation.New York, McGraw-Hill 646, 1966.
[23] Arkhipov, V.A., Bondarchuk, S.S., Zhukov, A.S., XXIX-th Siberian Thermalphysic Seminar: Proceedings of the All-Russian Conference, Institute of Thermal Physics SB RAS, 1–12 (2010).